Proceedings of Global Power and Propulsion Society
ISSN-Nr: 2504-4400
Beijing Conference 2019
16th – 18th September, 2019
www.gpps.global

GPPS-BJ-2019-0034

Numerical Study of Buoyancy-Driven Flow in a Closed Rotating Annulus

Feng Gao, John W. Chew
Thermo-fluid systems UTC,
Faculty of Engineering and Physical Sciences,
University of Surrey
f.gao@surrey.ac.uk, j.chew@surrey.ac.uk
Guildford, UK

Diogo B. Pitz
Faculty of Mechanical Engineering,
University of Campinas
diogopitz@gmail.com
Campinas, Brazil

ABSTRACT

This paper presents a numerical investigation of buoyancy-driven flow in a closed rapidly rotating disc cavity. Pseudo two-dimensional models are considered, with periodic boundary conditions on a thin axial domain. An incompressible model, in which density variation is considered with the Boussinesq approximation, is evaluated through comparisons with a full compressible model. Effects of property (viscosity) variation and dependency on buoyancy parameter ($\beta\Delta T$) and rotational Reynolds number for a given Rayleigh number, are investigated with the full compressible model. The mean centrifugal and radial Coriolis forces are analysed. Heat transfer predictions from the Boussinesq and compressible models agree to within 10%, for $\beta\Delta T \leq 0.2$.

INTRODUCTION

Economic and ecologic needs have driven manufacturers to design lower fuel consumption jet engines, by increasing by-pass ratios and overall pressure ratios. This requires smaller engine cores, and results in a proportionally larger compressor rotor blade tip clearance ratio, which must be controlled during different operating conditions across the engine cycle. The tip clearance of the compressor rotor blade is strongly dependent on the thermal growth of the compressor rotor discs, and in turn the heat transfer through the discs and the shroud. Efficient control of disc thermal growth requires clearer understanding on the mechanisms and reliable prediction tools of the flow within the rotor drum cavity.

An example of a compressor rotor disc cavity is given in Figure 1, reproduced from Fitzpatrick (2014). In this figure, open rotating cavities are formed between a shroud, discs and cobs. Axial throughflow, at the bore between the shaft and disc cobs, expected to cool the discs and shrouds which conduct heat generated by compression of gas in the main annulus flow. In some configurations radial inflow through the shroud may be used to cool the discs, or sealed cavities with no throughflow may occur.

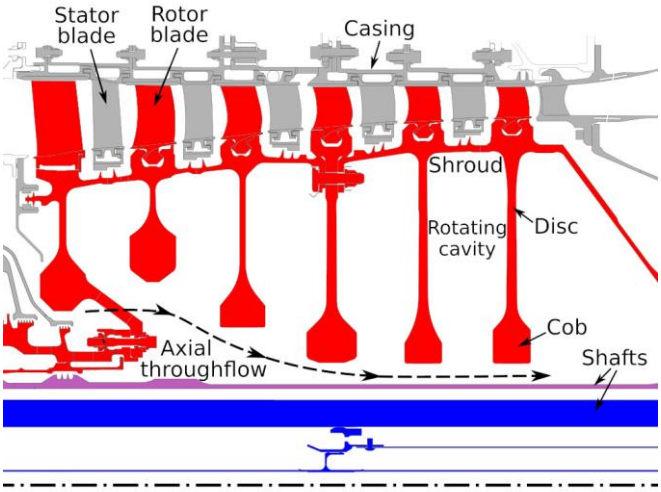

Figure 1 Cross Section of a Compressor Rotor Disc Cavity (Fitzpatrick, 2014)

The flow in rotating compressor cavities without radial throughflow is known to be buoyancy-driven, and usually has long time scale, i.e. it takes long time (compared to forced convection flows) to get to a steady state from a previous operating condition. This feature of the flow challenges both numerical predictions and experimental measurements. The understanding of the mechanisms of such flows has been reviewed by Owen and Long (2015). Some progress in understanding has been achieved, but researchers are still struggling in accurately simulating the buoyancy-driven flow inside the rotating cavities.

Recently, Pitz et al. (2019) reported, for the first time, statistics of the thermal and kinematic boundary layers in a sealed rotating cavity with heated shroud and cooled shaft. These were obtained from large-eddy simulation (LES). Inconclusive results have been obtained in comparing

predicted and measured shroud heat transfer. Pitz et al.'s (2019) predicted shroud Nusselt number agreed with the correlation for heat transfer between horizontal plates under gravity but not Bohn et al.'s (1995) results for a rotating cavity. However, Pitz et al. (2019) used an incompressible model and modelled the effect of density variation with Boussinesq approximation. This approach is well accepted for investigations of Rayleigh-Bénard convection under gravity but has not been validated for centrifugal buoyancy problems, in which centripetal acceleration is an additional factor.

The model considered by Pitz et al. (2019) is based on the experimental rig from Aachen University (Bohn et al., 1995). The definition of the Rayleigh number Ra (as used by Bohn et al.) is given in Eq. (1), where Pr is Prandtl number, $\beta\Delta T$ is the buoyancy parameter, Re_ϕ is the rotational Reynolds number, and a and b are the radii of the shaft and shroud. Further notation is defined in Figure 2 and the Nomenclature section at the end of the paper. For a given Ra there are infinite possible combinations of $\beta\Delta T$ and Re_ϕ. The rig operating condition was defined by a relation given in Eq. (2) for the configuration considered here, and a correlation was derived between the measured shroud Nusselt number (Nu) and Ra. However, the separate effect from $\beta\Delta T$ and Re_ϕ on shroud Nu is not clear.

$$Ra = 2Pr\beta\Delta T Re_\phi^2 \frac{b-a}{b+a} \quad (1)$$

$$Re_\phi = 1.441 Ra^{0.557} \quad (2)$$

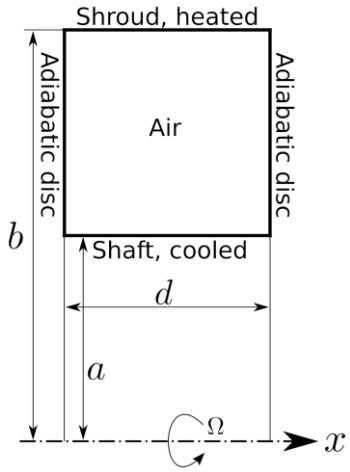

Figure 2 Illustration of Aachen University's Rig, Configuration B (Bohn et al., 1995)

The main aims of this paper are as follows.

(1) to investigate the validity of incompressible models with the Boussinesq approximation for centrifugal buoyancy-induced flow in a rapidly rotating disc cavity through comparisons with full compressible models,

(2) to understand the separate effect from $\beta\Delta T$ and Re_ϕ, and the effect of property variation (e.g. viscosity μ) on shroud Nu.

CONFIGURATION STUDIED

The geometry considered in this paper is configuration B of Bohn et al.'s (1995) rig, and as studied by Pitz et al. (2019). A schematic illustration of the geometry is given in Figure 2. This configuration is an air-filled closed annulus with geometric parameters a, b and d being 0.125m, 0.24m and 0.12m, respectively. The shroud is heated and the shaft is cooled. The two discs are considered as adiabatic. Shroud Nu were measured following the operating conditions defined by Eq. (2). A correlation between the measured shroud Nu and Ra was obtained, as given in Eq. (3). Later, Bohn and Gier (1998) noted that the discs were not perfectly adiabatic, and subsequently introduced a corrected version for the $Nu - Ra$ correlation, given in Eq. (4).

$$Nu = 0.317 Ra^{0.211} \quad (3)$$

$$Nu_{\text{corr}} = 0.0677 Ra^{0.297} \quad (4)$$

In this paper the configuration in Figure 2 is further simplified to a pseudo 2D test case, by shortening the axial extent of the model to $d = 10^{-4}$m and substituting no-slip discs with periodic boundary conditions. This very significantly reduced the computing requirements for the simulation. The 2D assumption not only removes any effect of the disc end walls, but restricts the turbulent motion. Although similar 2D assumptions have been used by others (King et al., 2005), some uncertainty regarding its effect must be acknowledged.

Test Matrix

The test matrix used for this study is summarised in Table 1. Parameters given in this table also include the Eckert number $Ec = \Omega^2 b^2/(Cp\Delta T)$. This is sufficiently small for the use of temperature transport equation as energy equation in the incompressible model to be considered appropriate. As well as rig condition tests, the matrix includes variation of $\beta\Delta T$ for $Ra = 3.3 \times 10^8$ and a fixed viscosity μ in the compressible model. Note that the same symbols as seen in Table 1 will be used in later plots. For all the tests statistics are collected over at least 50 rotor revolutions after a statistically steady state is reached. All the tests are run with direct numerical simulation (DNS), except the condition $Ra = 10^9$ for which Hydra employs large-eddy simulation (LES).

Table 1 Test Matrix

	Bohn et al.'s rig condition					
$\boldsymbol{Ra}$	10^7	10^8	10^9	3.3×10^8		
$\boldsymbol{\beta\Delta T}$	0.174	0.134	0.103	0.117	0.200	0.400
$\boldsymbol{10^{-4} Re_\phi}$	1.14	4.12	14.8	7.98	6.10	4.31
$\boldsymbol{10^3 Ec}$	0.0723	1.22	20.7	5.26	1.79	0.448
Semtex	△	△	△	△		□
Hydra varying μ	○	○	○	○	◇	◇
Hydra fixed μ						×

METHODOLOGY

The Navier-Stokes (N-S) equations are assumed to govern the problem described in this study. Numerical solutions were obtained using two codes, Hydra and Semtex.

Hydra

Hydra, owned by Rolls-Royce plc, is a full compressible N-S solver based on finite volume method with node-vertex unstructured meshes. A recent development (Amirante and Hills, 2015) extended Hydra to second order accuracy through linear reconstruction of primitive variables for flux estimation. The monotone upwind schemes for conservation laws based on a modified Roe scheme is used for spatial discretisation. The time interpolation employs an explicit 3-stage Runge-Kutta scheme. The working fluid is assumed to be air modelled as a perfect gas. The dynamic viscosity is calculated according to Sutherland's law.

Semtex

Semtex is an opensource spectral-element-Fourier code solving the incompressible form of the N-S equations (Blackburn and Sherwin, 2004). The finite element concept is applied on a basic 2D geometry and high-order Lagrange polynomials are implemented within each parametrically mapped quadrilateral element. Fourier expansions are applied to the third direction, which has to be homogenous. A semi-implicit second-order scheme (Karniadakis et al., 1991) is used for time discretisation.

In order to model centrifugal buoyancy-driven flow, the effect of density variation $\rho' = \rho - \rho_0$ must be considered in the centrifugal force term in the momentum equation as given below in Eq. (5).

$$\rho_0 \frac{\partial \vec{u}}{\partial t} + \rho_0 \vec{u} \cdot \nabla \vec{u} = -\nabla P + \rho_0 \nu \nabla^2 \vec{u} \underbrace{-2\rho_0 \vec{\Omega} \times \vec{u}}_{\text{Coriolis force term}} \underbrace{-\rho' \vec{\Omega} \times (\vec{\Omega} \times \vec{r})}_{\text{Cenrifugal buoyancy term}} \quad (5)$$

where P is the reduced pressure,

$$P = p + 0.5\rho_0 \left(\vec{\Omega} \times \vec{r}\right)^2$$

With the Boussinesq approximation, the density variation is neglected in all other terms. Density variation in the centrifugal buoyancy term is approximated, with

$$\rho' = -\beta(T - T_0)$$

where $\beta (= 1/T_\infty$, for a perfect gas) is the thermal expansion coefficient. The pressure is obtained by solving the Poisson equation, and the transport equation of temperature is considered as the energy equation.

Here we regard the N-S equation form as the primary difference between the two models. More details about the two solvers are given by (Amirante and Hills, 2015) and (Blackburn and Sherwin, 2004).

RESULTS AND DISCUSSION

Effect of Mesh Resolution

Mesh resolution studies have been conducted for all the operating conditions considered in this paper. An example is given for the Hydra solution with $Ra = 10^8$. Table 2 shows the effect of mesh resolution on shroud Nu and averaged core temperature. Figure 3 shows how the mesh resolution affects the flow field. At non-dimensional time $t = \tau$, the fine mesh solution is interpolated to the coarse mesh and solutions are continued on both meshes. After two rotor revolutions (at $t = \tau + 4\pi$) the "plumes" in the coarse mesh solution are more diffused, and under-prediction of the shroud Nu is seen in Table 2. The grid resolutions used in all subsequent results in this paper are given in Table 3. In the axial direction three mesh nodes are used in Hydra, and the axial plane number in Semtex is polynomial order plus one.

Table 2 Effect of Mesh Resolution on Hydra Solution for $Ra = 10^8$

Mesh	Δ_{wall}[mm]	N_r	N_θ	Nu	$\overline{T^*_{core}}$
Coarse	0.4	61	401	22.10	0.6416
Medium	0.2	101	801	23.03	0.6333
Fine	0.05	121	1201	23.11	0.6346

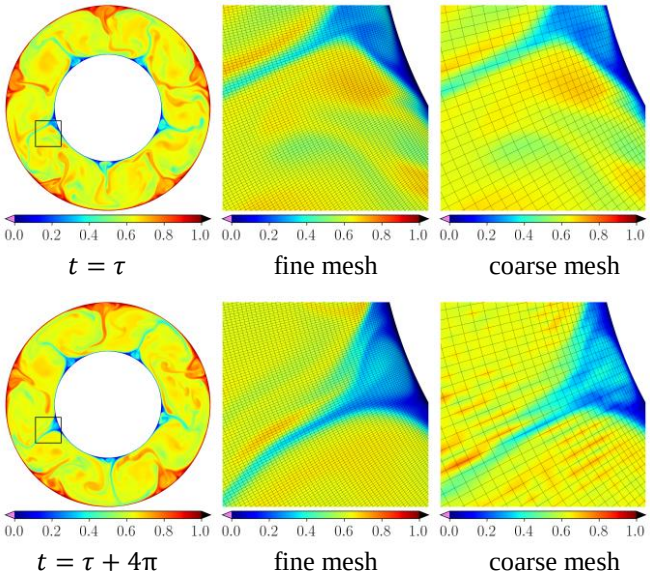

Figure 3 Mesh Resolution Effect on the Hydra Solutions for $Ra = 10^8$. (Rotor Revolution Time=2π)

Table 3: Mesh Information of the Test Cases Studied. Δ_{wall}, Near Wall Grid Height; N_r, Radial Grid Node Number; N_θ, Tangential Grid Node Number; N_{tot}, Total Grid Node Number; N_{el}, Number of Elements; P, Polynomial Order.

Hydra					
Ra	Δ_{wall}[mm]	N_r	N_θ	N_{tot}	Mode
10^7	0.2	101	801	~0.08M	DNS
10^8	0.1	121	1201	~0.15M	DNS
3.3×10^8	0.05	141	1401	~0.20M	DNS
10^9	0.03	121	1001	~0.12M	LES
Semtex					
Ra	Δ_{wall}[mm]	N_{el}	P	N_θ	N_{tot}
10^7	0.036	16	10	256	~0.04M
10^8	0.023	40	5	1024	~0.20M
3.3×10^8	0.023	40	5	1024	~0.20M
10^9	0.023	40	5	1600	~0.32M

Instantaneous Flow Field

Examples of the instantaneous temperature fields obtained with Semtex, and normalised as $T^* = (T - T_a)/(T_b - T_a)$, are given in Figure 4. Five pairs of cold/hot plumes or arms are observed for all the three conditions illustrated, and the flow state becomes more chaotic as Ra increases. At low Ra value strong arms penetrate through the core, driving the heat exchange. At high Ra value the arms are less visible, with shed vortices transporting heat between the shaft and shroud. Similar flow features and trends were observed in the Hydra solutions.

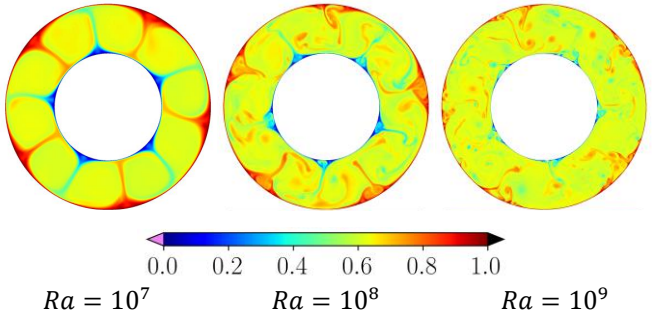

Figure 4 Normalised Instantaneous Temperature Field $T^*=(T - T_a)/(T_b - T_a)$, Obtained with Semtex.

Shroud Heat Transfer

The shroud Nusselt numbers predicted with both solvers are plotted against Ra in Figure 5, for Bohn et al.'s rig conditions. The graph also includes the correlation obtained from the rig by Bohn and co-workers (Bohn et al., 1995; Bohn and Gier, 1998), and a correlation acquired for heat convection between differentially heated horizontal plates under gravity by Hollands et al. (1975). The difference in Nu between the two codes is given, showing reasonable agreement, within a 10% threshold. The best agreement is observed at $Ra = 10^8$. Among the three correlations, the closest agreement with the predicted results is given by Bohn and Gier's corrected experimental correlation. It should be noted that some differences are seen in comparison with the 3D tests reported by Pitz et al. (2019), indicating further study is needed to investigate the effects of the disc boundary layers.

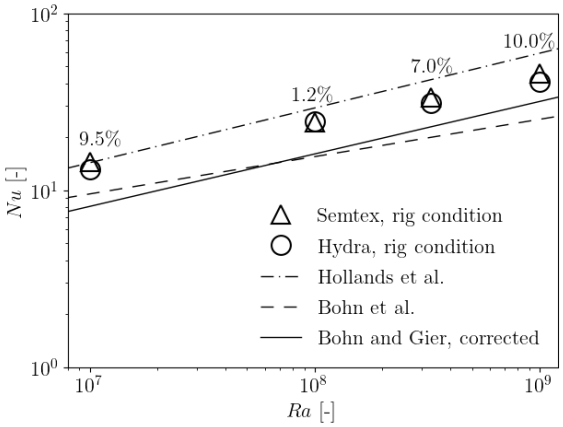

Figure 5 Shroud Nusselt Number versus Rayleigh Number. Comparison between Hydra and Semtex.

Shroud and Shaft Boundary Layers

The shroud and shaft boundary layers are considered in this section, again presenting results at Bohn et al.'s rig conditions. Mean values presented here have been averaged both in time and in the circumferential direction.

Thermal boundary layers

Mean temperature profiles are given in Figure 6. Both codes predict a uniform mean core temperature, and the boundary layer thins as Ra increases, agreeing with Pitz et al.'s (2019) observation. In Semtex solutions $\overline{T^*_{\text{core}}}$ is nearly invariant over the range of Ra considered. This differs from Pitz et al.'s (2019) 3D simulations, in which $\overline{T^*_{\text{core}}}$ increases slightly with Ra. For Hydra results a slight decrease of $\overline{T^*_{\text{core}}}$ is observed as Ra is increased.

Figure 7 shows the root mean square profiles of the temperature fluctuations. When Ra increases the T^*_{rms} peaks move toward the cylindrical surfaces, and the corresponding amplitudes reduce. This is observed in both solvers' results. Some slight differences may be seen in results from the two solvers, although trends are generally similar.

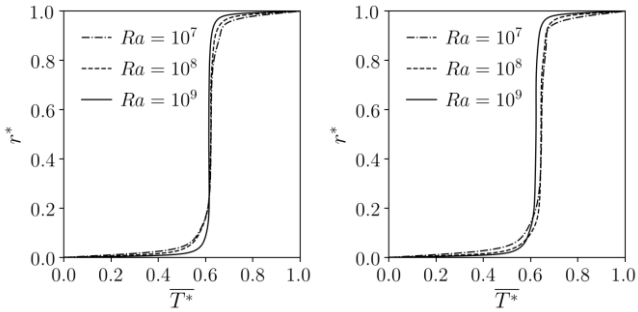

(a) Semtex (b) Hydra

Figure 6 Mean Temperature Profiles for Bohn et al.'s Rig Conditions, Averaged in Time and in the Tangential Direction

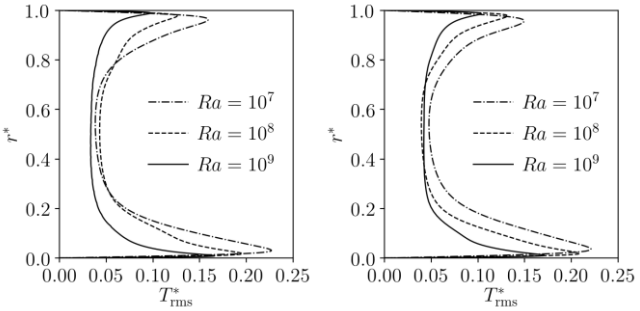

(a) Semtex (b) Hydra

Figure 7 Root Mean Square of Temperature Fluctuations for Bohn et al.'s Rig Conditions, Averaged in Time and in the Tangential Direction

Kinematic boundary layers

The simulations are run in a relative frame of reference rotating with the rig and the mean flow is close to solid body rotation. Hence, the velocity fluctuation profiles are plotted

here to investigate the kinematic boundary layer. The root mean squares of v_θ are shown in Figure 8, with different normalisations (Ωa and $\Omega a\sqrt{\beta\Delta T}$). Two peaks are observed near the cylindrical surfaces. In subplot (a) stronger peak values are given by low Ra condition. Taking $\Omega a\sqrt{\beta\Delta T}$ to scale the velocity fluctuations, as shown in subplot (b), reasonably good agreement of the curves is achieved, particularly for the peak amplitudes. This suggests that $\Omega a\sqrt{\beta\Delta T}$ is an appropriate velocity scale, as might be expected from the form of the driving centrifugal buoyancy force. However, this scale is not that successful in correlating the radial velocity fluctuations, as shown in Figure 9.

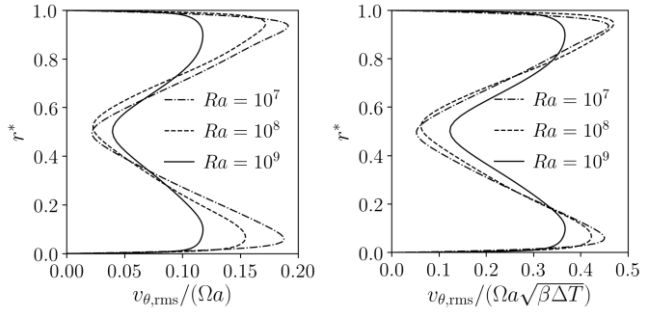

(a) (b)

Figure 8 Root Mean Square of Tangential Velocity Fluctuations for Bohn et al.'s Rig Conditions, Obtained with Hydra, Averaged in Time and in the Tangential Direction. (a) Normalised with Ωa; (b) Normalised with $\Omega a\sqrt{\beta\Delta T}$

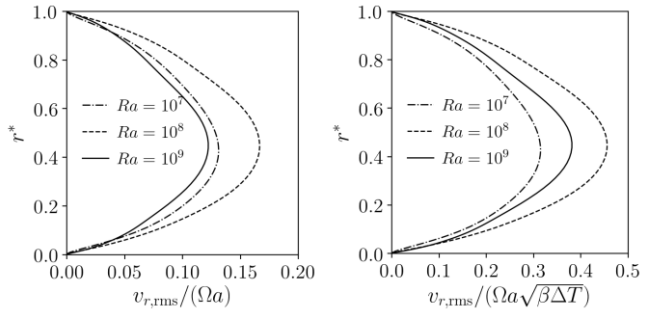

(a) (b)

Figure 9 Root Mean Square of Radial Velocity Fluctuations for Bohn et al.'s Rig Conditions, Obtained with Hydra, Averaged in Time and in the Tangential Direction. (a) Normalised with Ωa; (b) Normalised with $\Omega a\sqrt{\beta\Delta T}$

Effect of $\beta\Delta T$ for a Given Rayleigh Number

From the definition in Eq. (1), it is clear that a given Ra can be achieved by different combinations of $\beta\Delta T$ and Re_ϕ. Figure 10 shows how the buoyancy parameter $\beta\Delta T$ affects the shroud Nu for Ra fixed at 3.3×10^8. No distinguishable difference is observed with Semtex solutions. Hydra results show the shroud Nu decreases with the increase of $\beta\Delta T$ at high $\beta\Delta T$ values. This is similar to the behaviour expected in gravitational convection where the Boussinesq approximation is typically assumed to hold for $\beta\Delta T \leq 0.2$.

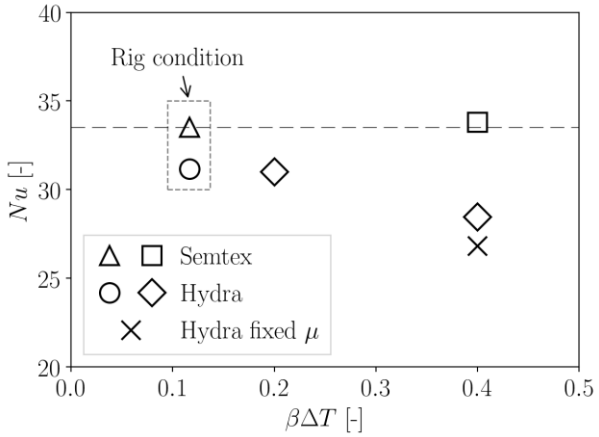

Figure 10 Shroud Nu for $Ra = 3.3\times10^8$, Obtained from Both Hydra and Semtex

The profiles of the thermal boundary layers are shown in Figure 11. Some effects of $\beta\Delta T$ can be observed through the mean core temperature, and differences in the temperature fluctuations are just visible. Figure 12 plots the profiles of kinematic boundary layers. The profiles are normalised with $\Omega a\sqrt{\beta\Delta T}$. Here use of this parameter helps to collapse the plots of both the tangential and radial velocities.

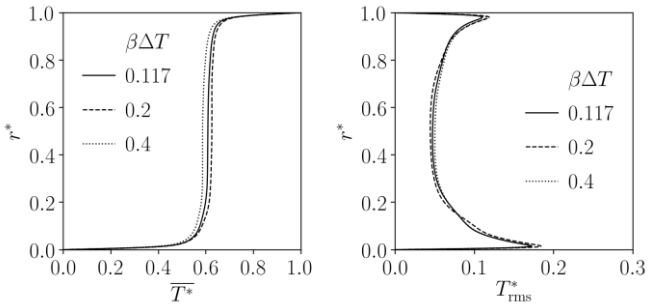

Figure 11 Mean Temperature and RMS of Temperature Fluctuations Profiles, Obtained with Hydra, $Ra = 3.3\times10^8$

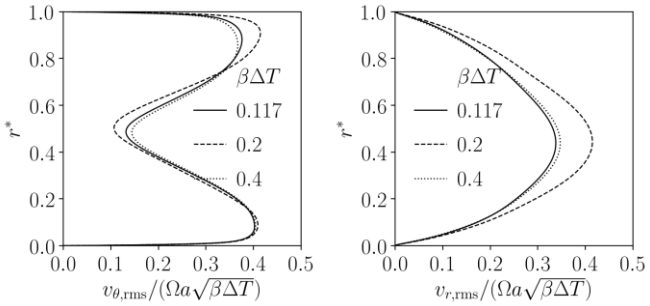

Figure 12 RMS of Tangential and Radial Velocity Fluctuations, Obtained with Hydra, $Ra = 3.3\times10^8$.

Effect of Property Variation

The fluid viscosity and thermal conductivity are known to vary with temperature, while these properties are treated as constants in the incompressible solver. A simulation was conducted in Hydra fixing the dynamic viscosity throughout the computational domain with $Ra = 3.3\times10^8$ and

$\beta\Delta T = 0.4$. A comparison with the varying viscosity test case at the same operating condition is shown in Figure 10 for shroud Nu. As the dynamic viscosity is fixed a smaller Nu is obtained. The effect is very limited compared with the influence of $\beta\Delta T$ or Ra. For the profiles of thermal and kinematic boundary layers, the effect from fixing viscosity is considered negligible.

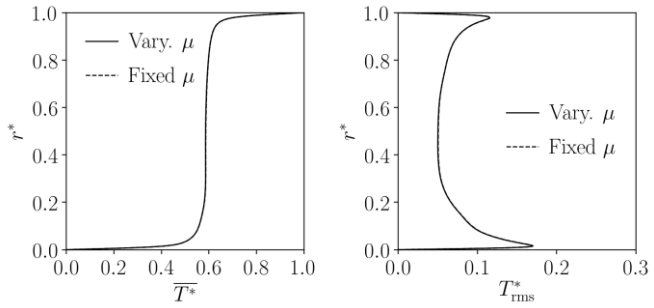

Figure 13 Mean Temperature and RMS of Temperature Fluctuations Profiles, $Ra = 3.3 \times 10^8$, with Viscosity and Fixed Viscosity, Obtained from Hydra

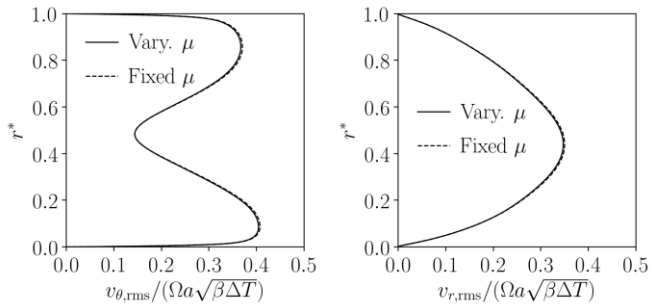

Figure 14 RMS of Tangential and Radial Velocity Fluctuations, Obtained from Hydra. $Ra = 3.3 \times 10^8$, with Varying Viscosity and Fixed Viscosity

Centrifugal and Coriolis Forces

The importance of Coriolis force in centrifugal buoyant flows in developing cyclonic and anti-cyclonic circulations for heat transport between the shaft and shroud has been emphasised by Owen and Long (2015). This force differentiates the present problem from natural heat convection between horizontal plates under gravity. The radial Coriolis force is induced by the relative circumferential flow motions and can act as a restoring force to weaken the heat transfer in the radial direction due to the centrifugal buoyancy force. Equation (6) gives the expressions of non-dimensional averaged centrifugal and radial Coriolis force terms from the compressible momentum equation in Hydra.

$$f_{\mathrm{cen}} = (\langle\rho\rangle - \langle\rho_{\mathrm{core}}\rangle)\Omega^2 r/(\langle\rho_{\mathrm{core}}\rangle\Omega^2 a)$$
$$f_{\mathrm{Cor}} = 2\langle\rho v_\theta\rangle\Omega/(\langle\rho_{\mathrm{core}}\rangle\Omega^2 a) \qquad (6)$$

Figure 15 shows the centrifugal and radial Coriolis force for Bohn et al.'s rig conditions, obtained with Hydra. In the core the centrifugal forces are zero, corresponding to the uniform mean core temperatures. Close to the cylindrical surfaces large centrifugal forces are observed. These reduce with the increase of Ra, associated with the decrease of $\beta\Delta T$. The radial Coriolis forces show high values in the core and develop gradually to zero towards the cylindrical surfaces. Therefore, the flow is dominated by centrifugal buoyancy force near the shroud and shaft where the principal resistance to heat transfer occurs. This suggests Coriolis forces have little effect on overall heat transfer, contrasting with experimental and some numerical results that show lower average heat transfer than expected from gravitational convection correlations. This behaviour is being further investigated with full 3D simulations.

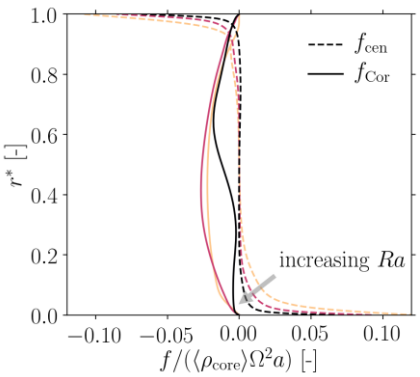

Figure 15 Centrifugal and Radial Coriolis Forces for Rig Conditions, Obtained with Hydra.

CONCLUDING REMARKS

Numerical studies have been conducted for buoyancy-driven flows in a closed rapidly rotating cavity using pseudo 2D models. Solvers for compressible and incompressible Navier-Stokes equations are considered. The incompressible solver employs the Boussinesq approximation in the centrifugal buoyancy term to consider the effect of density variation.

The study of mesh resolution effect with Hydra's solutions shows how coarse meshes can weaken the "plumes", thus under-predicting heat transfer.

Reasonably good agreement, within 10%, is achieved for shroud Nusselt number between the two solvers. Reasonably good agreement is also obtained, between the two solvers, for the thermal boundary layers. An invariant uniform mean core temperature is predicted by Semtex, differing from the 3D simulations by Pitz et al. (2019). Hydra shows uniform mean core temperatures but with temperature decreasing with the increase of Ra.

Regarding the kinematic boundary layers, the tangential velocity scales approximately with the parameter $\Omega a\sqrt{\beta\Delta T}$. But this does not apply to the radial velocity for the rig conditions considered.

Increasing $\beta\Delta T$ while at fixed Ra, Semtex gave negligible change in shroud Nu, whereas Hydra shows noticeable shroud Nu reduction. This indicates the validity of the Boussinesq approximation weakens as $\beta\Delta T$ increases. Using a constant dynamic viscosity reduced slightly the shroud Nu. Note, however, that the variation of shroud Nu for the conditions investigated ($Ra = 3.3 \times 10^8$,

$\beta\Delta T \leq 0.4$) is rather small compared with that produced by changing Ra.

For a fixed Ra in Hydra, slight variation of mean core temperature was observed as $\beta\Delta T$ changes. Both the tangential and radial velocities scaled approximately with the parameter $\Omega a\sqrt{\beta\Delta T}$. Hydra solutions also show negligible differences on the thermal and kinematic boundary layers between varying and fixed viscosity.

The analysis of centrifugal and radial Coriolis forces from Hydra solutions suggests that the flow is dominated by the centrifugal force near the cylindrical surfaces, where the main resistance to heat transfer occurs.

Further study will consider full 3D simulations.

NOMENCLATURE

Roman symbols

a, b	Radii of the shaft and shroud
Ec	Eckert number $Ec = \Omega^2 b^2/(C_p\Delta T)$
f_{cen}	Centrifugal force
f_{Cor}	Coriolis force
Nu	Shroud Nusselt number, ratio of convective heat flux to natural heat conduction
Pr	Prandtl number
r^*	Normalised radius $r^* = (r-a)/(b-a)$
Ra	Rayleigh number $Ra = 2Pr\beta\Delta T Re_\phi^2 \frac{b-a}{b+a}$
Re_ϕ	Rotational Reynolds number $Re_\phi = \frac{\rho\Omega(b+a)(b-a)}{2\mu}$
t	Non-dimensional time $t = \text{time}/\Omega$
T^*	Normalised temperature $T^* = (T - T_a)/\Delta T$
$\overline{T^*}$	Mean temperature, averaged in time and the tangential direction
T^*_{rms}	Root mean square of temperature fluctuations
$v_{r,\text{rms}}$	Root mean square of radial velocity
$v_{\theta,\text{rms}}$	Root mean square of tangential velocity

Greek symbols

β	Thermal expansion coefficient $\beta = 1/(T_a + T_b)$
$\beta\Delta T$	Buoyancy parameter
ΔT	Temperature difference between shroud and shaft $\Delta T = T_b - T_a$
μ	Dynamic viscosity
Ω	Angular speed
ρ	Fluid density

Subscripts

core	Value at the core

ACKNOWLEDGMENTS

The project is supported by the Engineering and Physical Science Research Council (Grant EP/P004091/1). The computing resources are provided by ARCHER and local clusters in the University of Surrey. We would like to acknowledge Rolls-Royce plc for permission to use the Hydra solver.

REFERENCES

Amirante, D. and Hills, N.J. (2015). Large-eddy simulations of wall bounded turbulent flows using unstructured linear reconstruction techniques. Journal of Turbomachinery, 137(5):051006. doi:10.1115/1.4028549

Blackburn, H.M. and Sherwin, S.J. (2004). Formulation of a Galerkin spectral element–Fourier method for three-dimensional incompressible flows in cylindrical geometries. Journal of Computational Physics, 197(2):759-778. doi: 10.1016/j.jcp.2004.02.013

Bohn, D., Deuker, E., Emunds, R. and Gorzelitz, V. (1995). Experimental and theoretical investigations of heat transfer in closed gas-filled rotating annuli. Journal of turbomachinery, 117(1):175-183. doi:10.1115/1.2835635

Bohn, D., and Gier, J. (1998). The effect of turbulence on the heat transfer in closed gas-filled rotating annuli for different Rayleigh numbers. In Proceedings of ASME 1998 International Gas Turbine and Aeroengine Congress and Exhibition, 1998. Paper No. 98-GT-542. doi:10.1115/98-GT-542

Fitzpatrick, J.N. (2014). Coupled thermal-fluid analysis with flowpath-cavity interaction in a gas turbine engine. Master thesis, Purdue University.

Hollands, K.G.T., Raithby, G.D. and Konicek, L. (1975). Correlation equations for free convection heat transfer in horizontal layers of air and water. International Journal of Heat and Mass Transfer, 18(7-8):879-884. doi: 10.1016/0017-9310(75)90179-9

Karniadakis, G.E., Israeli, M. and Orszag, S.A. (1991). High-order splitting methods for the incompressible Navier-Stokes equations. Journal of computational physics, 97(2):414-443. doi: 10.1016/0021-9991(91)90007-8

King, M.P., Wilson, M. and Owen, J.M. (2005). Rayleigh-Bénard convection in open and closed rotating cavities. Journal of engineering for gas turbines and power, 129(2):305-311. doi: 10.1115/1.2432898

Owen J.M. and Long C.A. (2015). Review of buoyancy-induced flow in rotating cavities. Journal of Turbomachinery, 137(11):111001. doi:10.1115/1.4031039

Pitz, D.B., Chew, J.W. and Marxen, O. (2019). Large-eddy simulation of buoyancy-induced flow in a sealed rotating cavity. Journal of Engineering for Gas Turbines and Power, 141(2):021020. doi:10.1115/1.4041113